ISSN 1070-3284, Russian Journal of Coordination Chemistry, 2023, Vol. 49, No. 1, pp. 10–23. © Pleiades Publishing, Ltd., 2023.
Russian Text © The Author(s), 2023, published in Koordinatsionnaya Khimiya, 2023, Vol. 49, No. 1, pp. 13–26.

Species of Gold(III) Binding by Binuclear Zinc Dipropyldithiocarbamate: Supramolecular Self-Organization and Thermal Behavior of Ionic Complexes $[Au(S_2CNPr_2)_2]_2[ZnCl_4]$ and $[Au(S_2CNPr_2)_2]_2[AuCl_4][AuCl_2]$

O. V. Loseva[a], T. A. Rodina[b], A. V. Gerasimenko[c], and A. V. Ivanov[a, *]

[a] *Institute of Geology and Nature Management, Far Eastern Branch, Russian Academy of Sciences, Blagoveshchensk, Russia*
[b] *Amur State University, Blagoveshchensk, Russia*
[c] *Institute of Chemistry, Far Eastern Branch, Russian Academy of Sciences, Vladivostok, Russia*
**e-mail: alexander.v.ivanov@chemist.com*

Received April 4, 2022; revised April 27, 2022; accepted April 29, 2022

Abstract—The reaction of binuclear zinc dipropyldithiocarbamate $[Zn_2\{S_2CN(C_3H_7)_2\}_4]$ with an $AuCl_3$/2 M HCl solution is studied. The double ionic complex $[Au\{S_2CN(C_3H_7)_2\}_2]_2[ZnCl_4]$ (**I**) is identified as the main species of gold(III) binding in the heterogeneous system under study and is characterized by ^{13}C and ^{15}N CP-MAS NMR spectroscopy. Single crystals of heterovalent compound $[Au\{S_2CN(C_3H_7)_2\}_2]_2[AuCl_4][AuCl_2]$ (**II**) are sampled as a by-product. The crystal and supramolecular structures of complexes **I** and **II** are determined by the direct XRD method (CIF files CCDC nos. 2159171 and 2159170, respectively). The self-organization of the complex pseudopolymeric structures of compounds **I** and **II** are shown to be due to the binding of ionic structural units by secondary nonvalent interactions Au···S and S···Cl and hydrogen bonds C–H···Cl. The thermal behavior of the complexes is studied by simultaneous thermal analysis (STA), and the quantitative regeneration of bound gold (**I** and **II**) with the partial transformation of released $ZnCl_2$ to ZnS (**I**) is found.

Keywords: zinc dialkyldithiocarbamates, double gold(III)–zinc complexes, heterovalent gold(III)–gold(I) complexes, supramolecular self-organization, secondary Au···S and S···Cl interactions, C–H···Cl hydrogen bonds, ^{13}C and ^{15}N CP-MAS NMR, thermal behavior

DOI: 10.1134/S1070328422700233

INTRODUCTION

Dithiocarbamates formed by the majority of metals are characterized by an exclusive structural diversity (for the systematization and detailed discussion of structural organization types of zinc dithiocarbamates, see [1]). The zinc complexes with the dithiocarbamate ligands are of considerable interest because of possibilities of practical using as analytical reagents [2], fungicides [3–5], catalysts [6, 7], corrosion inhibitors [8], vulcanization accelerators [9–11], and others. Owing to high volatility, they are also convenient precursors in the preparation of semiconducting nanopowders and ZnS [12–15] and ZnO [16] films (used in electronic industry) by chemical vapor deposition methods. Since the toxicity of zinc dithiocarbamates is low, their biological activity, including immunoregulatory, antioxidant, antibacterial, and antitumor properties, is intensely studied [17–21]. The use of this class of compounds also seems promising for the treatment of HIV infection: the therapeutic effect is achieved due to the inhibition of the nuclear factor with the weakening of HIV symptoms, enhancement of the immune function of the organism, and retardation of HIV progress to AIDS [22–24].

The previous study of the chemisorption properties of zinc dithiocarbamates established their capability of efficiently binding gold(III) from acidic solutions to form a whole series of pseudopolymeric dithiocarbamato-chlorido compounds with complicatedly organized supramolecular architectures, including heteronuclear Au(III)–Zn complexes [25–29], homonuclear Au(III) complexes [26, 30, 31], and heterovalent Au(III)–Au(I) complexes [25, 30].

The reaction of binuclear dipropyldithiocarbamate (Pr_2Dtc) of zinc, $[Zn_2\{S_2CN(C_3H_7)_2\}_4]$, with an $AuCl_3$/2 M HCl solution was studied in this work. An ionic dithiocarbamato-chlorido complex $[Au\{S_2CN(C_3H_7)_2\}_2]_2[ZnCl_4]$ (**I**) was isolated as the major individual species of gold binding from the studied heterogeneous system and characterized in detail using ^{13}C and ^{15}N CP-MAS NMR spectroscopy.

In addition, a minor number of crystals of the accompanying heterovalent gold compound of $[Au\{S_2CN(C_3H_7)_2\}_2]_2[AuCl_4][AuCl_2]$ (**II**) was sampled. The direct XRD method was used to determine the crystal and supramolecular structures of the synthesized Au(III)–Zn and Au(III)–Au(I) complexes. Studying the thermal behavior of compounds **I** and **II** by the STA technique, elemental gold (in the cases of **I** and **II**) and its accompanying zinc sulfide (in the case **II**) were identified as the end-products generated during the thermolysis.

EXPERIMENTAL

Sodium dipropyldithiocarbamate was synthesized by the reaction of carbon disulfide (Merck) and dipropylamine (Merck) in an alkaline medium [32]. The original binuclear zinc dipropyldithiocarbamate $[Zn_2\{S_2CN(C_3H_7)_2\}_4]$ (earlier characterized by XRD [33] and ^{13}C and ^{15}N CP-MAS NMR spectroscopy [34]) was synthesized by precipitation from the aqueous phase using the reaction between solutions of $ZnSO_4 \cdot 7H_2O$ (Sigma-Aldrich) and $Na\{S_2CN(C_3H_7)_2\} \cdot H_2O$ taken in the stoichiometric ratio.

Synthesis of complex I. Double pseudopolymeric bis(*N*,*N*-dipropyldithiocarbamato-*S*,*S*')gold(III) tetrachlorozincate(II) (**I**) was synthesized by the reaction of freshly precipitated zinc dipropyldithiocarbamate with an $AuCl_3$/2 M HCl solution

$$[Zn_2(S_2CNPr_2)_4] + 2H[AuCl_4]$$
$$= [Au(S_2CNPr_2)_2]_2[ZnCl_4] + ZnCl_2 + 2HCl.$$

A solution (10 mL) of $H[AuCl_4]$ containing gold (47.1 mg) was added dropwise to the white curd precipitate of $[Zn_2\{S_2CN(C_3H_7)_2\}_4]$ (100 mg), and the mixture was magnetically stirred for 1 h. On contact with a solution of $H[AuCl_4]$, the color of the precipitate of the zinc complex rapidly changes to yellow-orange with the gradual formation of a compact plastic mass, which transformed into a finely crystalline powder upon thorough trituration in water with a glass stick. The formed powder was washed with water on a filter and dried. The yield of compound **I** was 93.4%.

Crystals of compound **I** (transparent, yellow, flattened square prismatic) suitable for XRD were obtained by the dissolution of the prepared powder in acetone on moderate heating followed by the slow evaporation of the solvent at room temperature.

For $C_{28}H_{56}N_4S_8Cl_4ZnAu_2$ (**I**)

Anal. calcd., %:	C, 25.74;	H, 4.32;	N, 4.29
Found, %:	C, 25.74;	H, 4.56;	N, 4.39

IR for **I** (ν, cm^{-1}): 3670, 2964, 2929, 2874, 1548, 1444, 1343, 1304, 1252, 1183, 1149, 1081, 1046, 959, 893, 749, 637, 601, 557.

$^{13}C//^{15}N$ CP-MAS NMR of **I** (δ, ppm): 197.6, 196.9, 194.5, 191.5 (1 : 1 : 1 : 1, $-S_2\mathbf{C}N<$); 59.5, 57.6, 56.9, 55.7, 55.3 (1 : 1 : 1 : 3 : 2, $>NCH_2-$); 23.4, 23.1, 22.7, 22.2, 21.5, 20.9 (1 : 1 : 1 : 3 : 1 : 1, $-CH_2-$); 13.6, 13.3, 13.0, 12.5, 12.1, 11.6 (2 : 1 : 1 : 1 : 2 : 1, $-CH_3$) // 159.7, 155.2, 151.4, 149.3 (1 : 1 : 1 : 1, $-S_2C\mathbf{N}<$).

Single elongated prismatic crystals of bis(*N*,*N*-dipropyldithiocarbamato-*S*,*S*')gold(III) dichloroaurate(I)-tetrachloroaurate(III) (**II**; the amount of crystals of this type did not exceed 5% of the total amount) were taken from the overall mass of the crystallized substance. The formation of compound **II** can be explained as follows:

(1) some amount of $H[AuCl_4]$ still remains in the solution after the formation of a compact mass of complex **I** (see above), which results in a possibility for an additional gold(III) binding at the interface

$$1/2[Au(S_2CNPr_2)_2]_2[ZnCl_4] + H[AuCl_4]$$
$$= [Au(S_2CNPr_2)_2][AuCl_4] + 1/2\,ZnCl_2 + HCl;$$

(2) in turn, the subsequent crystallization of the additionally formed gold(III) complex is accompanied by the reduction of 50% $[AuCl_4]^-$ anions to $[AuCl_2]^-$ involving acetone [25, 35]

$$[AuCl_4]^- + CH_3COCH_3$$
$$= [AuCl_2]^- + CH_2ClCOCH_3 + HCl.$$

Elemental analysis was carried out on a Carlo Erba EA 1108 automated elemental analyzer. The IR spectrum was recorded on a Perkin-Elmer Spectrum 65 FT-IR spectrophotometer using the attenuated total internal reflectance (ATR) method in a frequency range of 400–4000 cm^{-1}.

The residual content of gold in the solution was determined on a Hitachi atomic absorption spectrometer (class 1, model 180-50). The degree of binding of gold from the solution to the solid phase was 97%.

XRD of single crystals of compounds **I** and **II** was carried out on a BRUKER Kappa APEX II diffractometer (MoK_α radiation, λ = 0.71073 Å, graphite monochromator) at 200(2) and 170(1) K, respectively. An X-ray absorption correction was applied by indices of the single crystal faces and equivalent reflections for compounds **I** and **II**, respectively. The structures were determined by a direct method and refined by least squares in the anisotropic approximation of non-hydrogen atoms. The positions of hydrogen atoms were calculated geometrically and included in refinement by the riding model. The population coefficients of randomly distributed carbon atoms in compound **I** were specified to be 0.6 and 0.4 for the atoms with indices *A* and *B*, respectively. The independent refinement of these coefficients gave the same values with the accuracy to 0.04. Data were collected and edited and unit cell parameters were refined using the APEX2 programs [36]. All calculations on structure

Table 1. Crystallographic data and experimental and structure refinement parameters for compounds $[Au\{S_2CN(C_3H_7)_2\}_2]_2[ZnCl_4]$ (**I**) and $[Au\{S_2CN(C_3H_7)_2\}_2]_2[AuCl_4][AuCl_2]$ (**II**)

Parameter	Value	
	I	**II**
Empirical formula	$C_{28}H_{56}N_4S_8Cl_4ZnAu_2$	$C_{28}H_{56}N_4S_8Cl_6Au_4$
FW	1306.35	1705.81
Crystal system	Monoclinic	Monoclinic
Space group	$P2_1/n$	$C2/c$
a, Å	14.9546(5)	32.6012(9)
b, Å	13.0269(4)	9.4225(2)
c, Å	24.1423(8)	17.7918(5)
β, deg	101.4520(10)	116.1910(10)
V, Å^3	4609.6(3)	4904.2(2)
Z	4	4
ρ_{calc}, g/cm^3	1.882	2.310
μ, mm^{-1}	7.486	12.623
F(000)	2544	3192
Crystal size, mm	0.43 × 0.39 × 0.28	0.46 × 0.20 × 0.14
Range of data collection over θ, deg	1.482–27.999	2.27–36.37
Ranges of reflection indices	$-19 \le h \le 14$, $-17 \le k \le 15$, $-31 \le l \le 29$	$-53 \le h \le 53$, $-15 \le k \le 15$, $-29 \le l \le 29$
Measured reflections	32351	74937
Independent reflections	11125 (R_{int} = 0.0246)	11818 (R_{int} = 0.0271)
Reflections with $I > 2\sigma(I)$	9504	10115
Refinement variables	522	245
GOOF	1.032	0.828
R factors for $F^2 > 2\sigma(F^2)$	R_1 = 0.0285, wR_2 = 0.0633	R_1 = 0.0198, wR_2 = 0.0416
R factors for all reflections	R_1 = 0.0378, wR_2 = 0.0678	R_1 = 0.0279, wR_2 = 0.0449
Residual electron density (min/max), e/Å^3	−0.849/1.823	−1.046/1.001

determination and refinement were performed using the SHELXTL programs [37, 38]. The atomic coordinates, bond lengths, and angles were deposited with the Cambridge Crystallographic Data Centre (CIF files CCDC nos. 2159171 (**I**) and 2159170 (**II**); deposit@ccdc.cam.ac.uk or http://www.ccdc.cam.ac.uk). Selected crystallographic data and structure refinement results for compounds **I** and **II** are given in Table 1. Selected bond lengths and angles for compounds **I** and **II** are listed in Table 2. The geometric parameters of hydrogen bonds in complex **II** are given in Table 3.

Solid-state $^{13}C/^{15}N$ CP-MAS NMR spectra were recorded on a CMX-360 spectrometer (Agilent/Varian/Chemagnetics InfinityPlus) with an operating frequency of 90.52/36.48 MHz, a superconducting magnet with B_0 = 8.46 T, and Fourier transform. A standard experiment of cross-polarisation (CP) from the protons together with proton decoupling for the suppression of ^{13}C-1H and ^{15}N-1H interactions were applied using the radiofrequency field at the resonance frequency of protons [39]. A sample of complex **I** (~80 mg) was placed in a 4.0-mm ZrO_2 ceramic rotor. For $^{13}C/^{15}N$ NMR measurements, the sample was rotated at the magic angle (MAS) with the spinning frequency at 5800(1)/6100(1) Hz, the acquisition number was 1300/21392, the duration of proton π/2 pulses was 4.9/4.7 μs, the $^1H-^{13}C/^1H-^{15}N$ contact time was 2.5/1.5 ms, and the interval between pulses was 3.0/2.0 s. The isotropic $\delta(^{13}C)/\delta(^{15}N)$ chemical shifts (ppm) are given relative to one of

Table 2. Selected bond lengths (*d*) and bond (ω) and torsion (φ) angles in the structures of compounds **I** and **II***

Compound **I**			
Bond	*d*, Å	Bond	*d*, Å
Au(1)–S(1)	2.3334(11)	S(6)–C(15)	1.741(4)
Au(1)–S(2)	2.3370(10)	N(3)–C(15)	1.298(5)
Au(1)–S(3)	2.3244(10)	N(3)–C(16)	1.478(6)
Au(1)–S(4)	2.3316(10)	N(3)–C(19A)	1.517(7)
Au(1)···S(8)	3.6714(12)	N(3)–C(19B)	1.542(9)
S(1)–C(1)	1.736(4)	Au(3)–S(7)	2.3318(10)
S(2)–C(1)	1.718(4)	Au(3)–S(8)	2.3391(11)
S(3)–C(8)	1.731(4)	Au(3)···S(4)	3.7257(11)
S(4)–C(8)	1.741(4)	S(7)–C(22)	1.733(4)
N(1)–C(1)	1.302(5)	S(8)–C(22)	1.737(4)
N(1)–C(2)	1.486(6)	N(4)–C(22)	1.303(5)
N(1)–C(5A)	1.544(8)	N(4)–C(23)	1.490(6)
N(1)–C(5B)	1.517(9)	N(4)–C(26)	1.479(6)
N(2)–C(8)	1.295(5)	Zn(1)–Cl(1)	2.3201(10)
N(2)–C(9A)	1.481(10)	Zn(1)–Cl(2)	2.2704(11)
N(2)–C(9B)	1.504(13)	Zn(1)–Cl(3)	2.2733(11)
N(2)–C(12)	1.468(6)	Zn(1)–Cl(4)	2.2672(13)
Au(2)–S(5)	2.3347(9)	S(2)[a]···Cl(3)[c]	3.3834(14)
Au(2)–S(6)	2.3265(10)	S(4)[a]···Cl(3)[c]	3.5045(16)
S(5)–C(15)	1.725(4)	S(5)···Cl(1)[c]	3.3349(15)
Angle	ω, deg	Angle	ω, deg
S(1)Au(1)S(2)	75.19(4)	S(5)Au(2)S(6)	75.66(4)
S(1)Au(1)S(3)	104.17(4)	C(15)N(3)C(16)	121.1(4)
S(1)Au(1)S(4)	177.54(5)	C(15)N(3)C(19A)	121.6(4)
S(2)Au(1)S(3)	176.89(4)	C(15)N(3)C(19B)	116.6(6)
S(2)Au(1)S(4)	105.05(3)	C(16)N(3)C(19A)	116.2(4)
S(3)Au(1)S(4)	75.73(4)	C(16)N(3)C(19B)	117.8(6)
S(1)Au(1)···S(8)	81.30(4)	S(7)Au(3)S(8)	75.09(4)
C(1)N(1)C(2)	122.0(4)	S(7)Au(3)S(8)[c]	104.91(4)
C(1)N(1)C(5A)	119.0(5)	S(7)[a]Au(3)···S(4)	73.32(3)
C(1)N(1)C(5B)	119.5(5)	C(22)N(4)C(23)	121.5(4)
C(2)N(1)C(5A)	117.2(5)	C(22)N(4)C(26)	120.8(4)
C(2)N(1)C(5B)	113.3(5)	C(26)N(4)C(23)	117.2(4)
C(8)N(2)C(12)	122.5(3)	Cl(1)Zn(1)Cl(2)	105.79(4)
C(8)N(2)C(9A)	124.6(11)	Cl(1)Zn(1)Cl(3)	108.91(4)
C(8)N(2)C(9B)	115.3(15)	Cl(1)Zn(1)Cl(4)	111.68(5)
C(12)N(2)C(9A)	112.7(11)	Cl(2)Zn(1)Cl(3)	110.37(5)
C(12)N(2)C(9B)	121.6(15)	Cl(2)Zn(1)Cl(4)	110.96(5)
S(5)Au(2)S(6)[b]	104.34(4)	Cl(3)Zn(1)Cl(4)	109.08(4)
Angle	φ, deg	Angle	φ, deg
Au(1)S(1)S(2)C(1)	174.7(3)	S(4)C(8)N(2)C(12)	3.2(6)
S(1)Au(1)C(1)S(2)	175.3(2)	Au(2)S(5)S(6)C(15)	−175.6(3)
S(1)C(1)N(1)C(2)	−178.6(4)	S(5)Au(2)C(15)S(6)	−176.1(2)
S(1)C(1)N(1)C(5A)	−14.3(7)	S(5)C(15)N(3)C(16)	2.6(8)
S(1)C(1)N(1)C(5B)	28.5(7)	S(5)C(15)N(3)C(19A)	−164.4(5)

Table 2. (Contd.)

Compound **I**			
Angle	ω, deg	Angle	ω, deg
S(2)C(1)N(1)C(2)	1.0(8)	S(5)C(15)N(3)C(19B)	158.3(6)
S(2)C(1)N(1)C(5A)	165.1(5)	S(6)C(15)N(3)C(16)	−178.0(4)
S(2)C(1)N(1)C(5B)	−152.0(5)	S(6)C(15)N(3)C(19A)	15.1(8)
Au(1)S(3)S(4)C(8)	−179.2(2)	S(6)C(15)N(3)C(19B)	−22.3(7)
S(3)Au(1)C(8)S(4)	−179.3(2)	Au(3)S(7)S(8)C(22)	176.4(2)
S(3)C(8)N(2)C(9A)	9.0(9)	S(7)Au(3)C(22)S(8)	176.8(2)
S(3)C(8)N(2)C(9B)	−6.2(2)	S(7)C(22)N(4)C(23)	−7.4(6)
S(3)C(8)N(2)C(12)	−175.7(3)	S(7)C(22)N(4)C(26)	−179.5(3)
S(4)C(8)N(2)C(9A)	−172.0(7)	S(8)C(22)N(4)C(23)	172.3(3)
S(4)C(8)N(2)C(9B)	172.8(1)	S(8)C(22)N(4)C(26)	0.2(6)
Compound **II**			
Bond	*d*, Å	Bond	*d*, Å
Au(1)–S(1)	2.3331(5)	N(2)–C(8)	1.311(2)
Au(1)–S(2)	2.3391(5)	N(2)–C(9)	1.470(3)
Au(1)–S(3)	2.3409(5)	N(2)–C(12)	1.470(3)
Au(1)–S(4)	2.3316(5)	Au(2)–Cl(1)	2.2874(5)
S(1)–C(1)	1.730(2)	Au(2)–Cl(2)	2.2786(6)
S(2)–C(1)	1.734(2)	Au(2)···S(1)	3.5302(6)
S(3)–C(8)	1.729(2)	Au(3)–Cl(3)	2.263(3)
S(4)–C(8)	1.725(2)	Au(3)–Cl(4)	2.268(3)
N(1)–C(1)	1.304(2)	S(2)[b]···Cl(1)	3.3200(8)
N(1)–C(2)	1.481(3)	S(3)[b]···Cl(1)	3.2835(9)
N(1)–C(5)	1.473(3)	S(4)···Cl(2)	3.3730(8)
Angle	ω, deg	Angle	ω, deg
S(1)Au(1)S(2)	75.447(18)	C(2)N(1)C(5)	117.11(16)
S(1)Au(1)S(3)	177.75(2)	C(8)N(2)C(9)	121.35(18)
S(1)Au(1)S(4)	103.762(18)	C(8)N(2)C(12)	120.88(18)
S(2)Au(1)S(3)	105.375(17)	C(9)N(2)C(12)	117.73(17)
S(2)Au(1)S(4)	178.01(2)	Cl(1)Au(2)Cl(2)	89.64(2)
S(3)Au(1)S(4)	75.346(18)	Cl(1)[a]Au(2)Cl(2)	90.36(2)
C(1)N(1)C(2)	121.68(18)	Cl(3)Au(3)Cl(4)	179.76(17)
C(1)N(1)C(5)	121.20(17)	Cl(2)Au(2)···S(1)	74.76(2)
Angle	φ, deg	Angle	φ, deg
Au(1)S(1)S(2)C(1)	179.33(8)	Au(1)S(3)S(4)C(8)	178.32(8)
S(1)Au(1)C(1)S(2)	179.40(7)	S(3)Au(1)C(8)S(4)	178.50(7)
S(1)C(1)N(1)C(2)	−4.7(2)	S(3)C(8)N(2)C(9)	−173.6(1)
S(1)C(1)N(1)C(5)	176.30(9)	S(3)C(8)N(2)C(12)	4.1(2)
S(2)C(1)N(1)C(2)	176.33(9)	S(4)C(8)N(2)C(9)	7.1(2)
S(2)C(1)N(1)C(5)	−2.6(2)	S(4)C(8)N(2)C(12)	−175.2(1)

* Symmetry transforms: [a] $-1/2+x, 1/2-y, 1/2+z$; [b] $1/2+x, 3/2-y, 1/2+z$; [c] $1/2-x, -1/2+y, 3/2-z$ (**I**); [a] $1/2-x, 3/2-y, 1-z$; [b] $1/2-x, 1/2-y, 1-z$ (**II**).

the components of the external standard: crystalline adamantane [40] (δ = 38.48 ppm relative to tetramethylsilane [41])/crystalline NH_4Cl (δ = 0.0 ppm, −341 ppm in the absolute scale with a correction to the magnetic field strength drift), the frequency equivalent of which was 0.051/0.018 Hz/h.

Table 3. Geometric parameters of hydrogen bonds in complex **II***

Contact D–H···A	Distance, Å			Angle D–H···A, deg
	D–H	H···A	D···A	
C(3)–H(3B)···Cl(2)[a]	0.99	2.91	3.829(2)	155
C(5)–H(5B)···Cl(3)[d]	0.99	2.81	3.704(3)	151
C(5)[e]–H(5B)[e]···Cl(4)[d]	0.99	2.97	3.786(3)	141
C(9)[f]–H(9A)[f]···Cl(3)[d]	0.99	2.90	3.707(3)	139
C(9)[b]–H(9A)[b]···Cl(4)[d]	0.99	2.79	3.656(3)	147

* Symmetry transforms: [a] $1/2 - x, 3/2 - y, 1 - z$; [b] $1/2 - x, 1/2 - y, 1 - z$; [d] $1/2 + x, -1/2 + y, z$; [e] $1 - x, 1 - y, 1 - z$; [f] $1/2 + x, 1/2 + y, z$.

Thermal behavior of compounds **I** and **II** was studied by the STA method on an STA 449C Jupiter instrument (NETZSCH) in corundum crucibles under a cap with a hole providing a vapor pressure of 1 atm during the thermal decomposition of the sample. The heating rate was 5°C/min to 1100°C under an argon atmosphere. The sample weights were 2.527–4.688 (**I**) and 2.070–5.313 (**II**) mg. The temperature measurement accuracy was ±0.6°C, and the weight change accuracy was $\pm 1 \times 10^{-4}$ mg. The correction file and temperature and sensitivity calibrations at the specified temperature program and heating rate were used when recording thermogravimetric (TG) and differential scanning calorimetry (DSC) curves. The melting points were independently determined on a PTP(M) instrument (OAO Khimlaborpribor, Russia).

After thermal analysis, the chemical composition of the residual substance was qualitatively carried out by the microprobe method using a RONTEC energy dispersive spectrometer integrated with a LEO-1420 scanning electron microscope.

RESULTS AND DISCUSSION

The high-intensity single absorption band observed in the IR spectrum of crystalline complex **I** at 1548 cm^{-1} is characteristic of stretching vibrations of the C–N bond in the dithiocarbamate groups >NC(S)S– [32, 43]. The intermediate position of the discussed value of ν(C–N) between the ranges of stretching vibrations of ordinary C–N (1250–1360 cm^{-1}) and double C=N (1640–1690 cm^{-1}) bonds and its substantial shift to the high-frequency range indicate the partially double character of the formally ordinary N–C(S)S bond [43, 44].

The medium-intensity absorption bands at 1149 and 959 cm^{-1} are assigned to asymmetric (ν_{as}) and symmetric (ν_s) stretching vibrations of the –C(S)S– group, respectively [43, 45]. The bands in a range of 557–749 cm^{-1} are due to the ν(C–S) vibrations [46]. The absorptions in a range of 2874–2964 cm^{-1} are attributed to stretching and bending vibrations of the alkyl substituent bonds in the Dtc ligands.

The ^{13}C CP-MAS NMR spectrum of complex **I** (Fig. 1a) exhibits four groups of resonance signals, whose chemical shifts (see above Synthesis of complex **I**) allow one to assign them to the structural positions of carbon in the chemical groups (>$NC(S)S$–, >NCH_2–, –CH_2–, and –CH_3) of the Pr_2Dtc ligand. Four ^{13}C signals of equal intensity in the range of dithiocarbamate groups indicate that the compound under study contains four structurally nonequivalent Pr_2Dtc ligands. In addition, the observed ratio of intensities of the ^{13}C resonance signals for each of the >NCH_2–, –CH_2–, and –CH_3 groups also indicates in favor of their nonequivalence in the adjacent chains of the alkyl substituents. The ^{15}N CP-MAS NMR data independently confirm the found nonequivalent character of the dithiocarbamate ligands (Fig. 1b). It is important that the $^{13}C/^{15}N$ chemical shifts of the >NC(S)S– groups lie in ranges of 191.5–197.6/149.3–159.7 ppm, which is completely consistent with the concept about the binding of the Pr_2Dtc ligands by gold in the form of cations $[Au(S_2CNPr_2)_2]^+$ [47, 48]. Obviously, the found structural nonequivalence of the Pr_2Dtc ligands (1 : 1 : 1 : 1) can be accomplished in one of the following variants: the presence in the structure of complex **I** of (a) four nonequivalent centrosymmetric gold(III) cations $[Au(S_2CNPr_2)_2]^+$, (b) two nonequivalent noncentrosymmetric cations, or (c) two nonequivalent centrosymmetric and two equivalent noncentrosymmetric cations. The direct XRD method was used to solve this alternative and determine the structural organization of the synthesized complexes.

The unit cell of each compound contains four formula units of complex **I** ($[Au\{S_2CN(C_3H_7)_2\}_2]_2[ZnCl_4]$) and **II** ($[Au\{S_2CN(C_3H_7)_2\}_2]_2[AuCl_4]$-

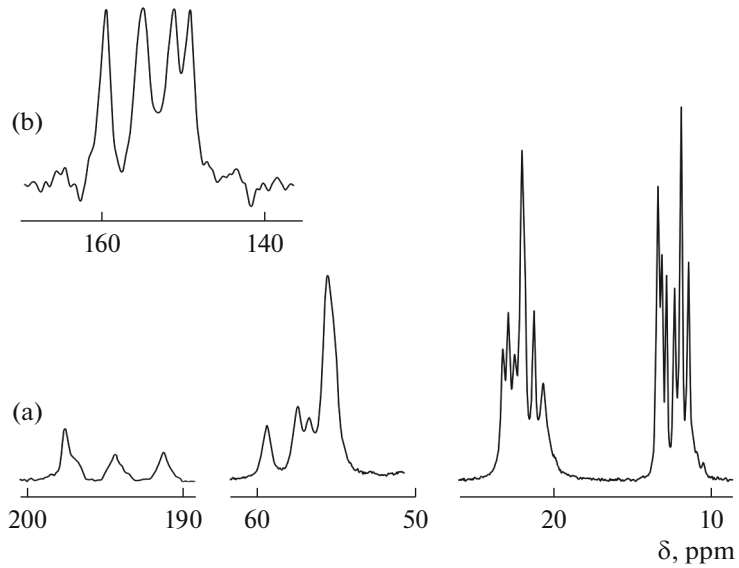

Fig. 1. The ^{13}C (a) and ^{15}N (b) CP-MAS NMR spectra of polycrystalline complex **I**; acquisition number/rotation frequency of the sample: (a) 1300/5.8 kHz and (b) 21 392/6.1 kHz.

$[AuCl_2]$) (Table 1, Fig. 2). As expected from the solid-state ^{13}C and ^{15}N CP-MAS NMR data, the cationic moiety of complex **I** contains three types of structurally nonequivalent complex cations $[Au(S_2CNPr_2)_2]^+$: noncentrosymmetric A with the Au(1) atom and centrosymmetric B (Au(2)) and C (Au(3)) in a ratio of 2 : 1 : 1 (Figs. 3a–3c). On the contrary, in compound **II**, the gold(III) complex cations are structurally unified and characterized by the noncentrosymmetric structure, including the nonequivalent Pr_2Dtc ligands (Fig. 4a). In the discussed cations of each of compounds **I** and **II**, the gold atom coordinates two Pr_2Dtc ligands in an *S*,*S*'-bidentate mode and forms planar chromophores $[AuS_4]$ (diagonal SAuS angles are equal or close to 180°), which is due to the low-spin intraorbital dsp^2 hybrid state of the central gold atom. The ligands in complexes **I** and **II** exhibit an almost isobidentate coordination character: the Au–S bond lengths lie in narrow ranges of 2.3244–2.3391 and 2.3316–2.3409 Å, respectively (Table 2).

It should be mentioned that the dithiocarbamate ligands in compounds **I** and **II** manifest a series of common properties. For example, the structure of the S_2CNC_2 groups appreciably deviate from the planar character (see the corresponding torsion angles in Table 2). The most significant deviation of the atoms from the coplanar arrangement is observed for cations A and B, whose Pr_2Dtc ligands contain the structurally disordered substituents $-C_3H_7$ (Figs. 3a, 3b). The N–C(S)S bonds (1.295–1.303/1.304, 1.311 Å) are substantially shorter than the N–CH_2 bonds (1.468–1.544/1.470–1.481 Å) and occupy an intermediate position between the ordinary C–N (1.47 Å) and double C=N (1.27 Å) bonds [49]. This fact indicates the partially double character of the N–C(S)S bonds caused by the mesomeric effect in the dithiocarbamate groups. The C–C bond lengths in the alkyl substituent lie in ranges of 1.413–1.525 and1.509–1.525 Å, respectively.

The result of the bidentate coordination of the ligands is the formation of two four-membered rings $[AuS_2C]$ bonded by the common gold atom. Small sizes of metallocycles are indicated by the Au···C (2.819–2.843/2.820, 2.826 Å) and S···S (2.845–2.859/2.856, 2.859 Å) distances that are significantly shorter than the sums of the van der Waals radii of the corresponding pairs of atoms: 3.36 and 3.60 Å, respectively [50]. The AuSSC and SAuCS torsion angles are close to 180°: the deviations are in ranges of 0.7°–5.3° and 0.60°–1.68° (Table 2) indicating the planar geometry of the metallocycles.

In spite of the substantial structural resemblance, nonequivalent cations A, B, and C in compound **I** exhibit reliable differences in the respective bond lengths, interatomic distances, and bond and torsion angles (Table 2), which allows us to classify them as conformers. The anionic moiety of complex **I** is presented by the distorted tetrahedral $[ZnCl_4]^{2-}$ anion containing four nonequivalent chlorine atoms (Fig. 3d). The ClZnCl bond angles, which lie in the range of 105.79–111.68° (Table 2), somewhat deviate from 109.5°, reflecting the sp^3 hybrid state of the central zinc atom. The parameter $\tau_4 = [360° - (\alpha + \beta)]/141°$ (where α and β are two largest LML angles) was used for the quantitative characterization of the

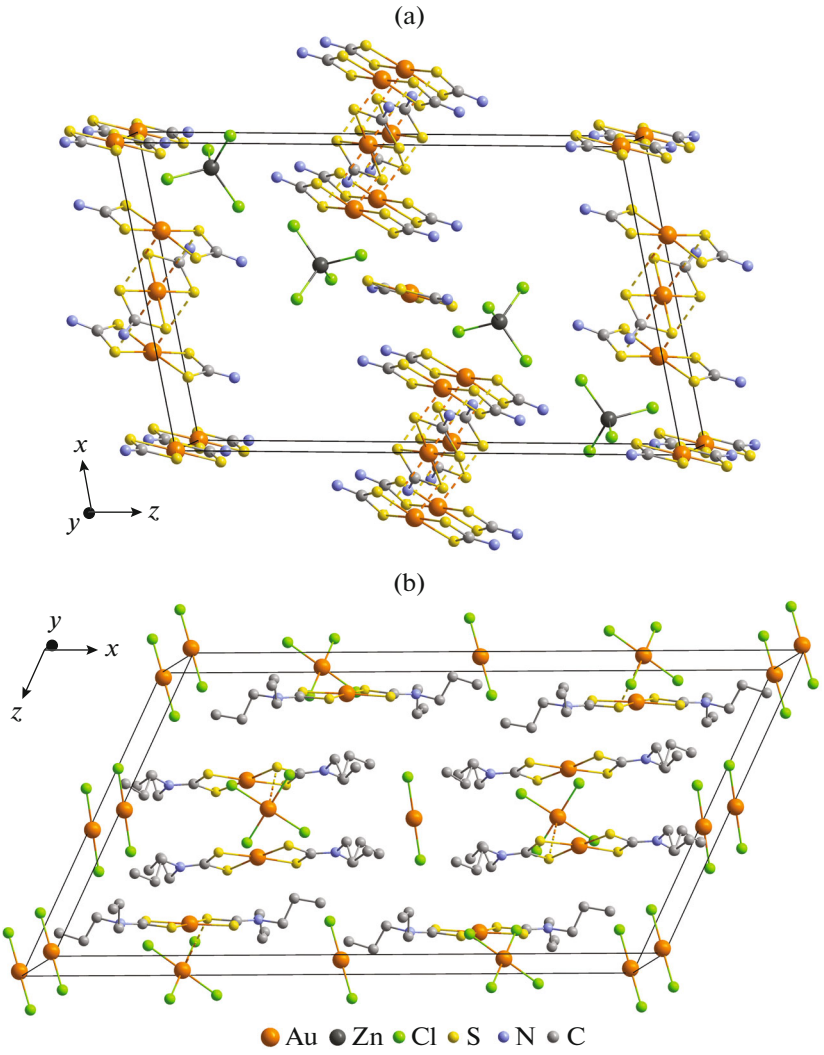

Fig. 2. Packing of the ionic structural units in the crystals of complexes (a) **I** and (b) **II**. For complex **I**, the alkyl substituents in the Pr_2Dtc ligands are omitted.

zinc polyhedron geometry [51]. The limiting values adopted by the τ_4 parameter, 0 ($\alpha = \beta = 180°$) and 1 ($\alpha = \beta = 109.5°$), correspond to the planar tetragonal and tetrahedral configurations of the polyhedra in the complexes having the fourfold coordination geometry. In our case, two largest LZnL angles, 111.68° and 110.96° (Table 2), specify the parameter $\tau_4 = 0.974$, which indicates the predominant (97.4%) contribution of the tetrahedral component to the geometry of the zinc polyhedron.

Compound **II** contain the noncentrosymmetric gold(III) cations and heterovalent gold anions: centrosymmetric $[AuCl_4]^-$ of the square-planar structure (dsp^2 hybrid state of the central atom) and linear noncentrosymmetric $[AuCl_2]^-$ (sp hybridization) (Figs. 4b, 4c).

The supramolecular level of the structural self-organization of complex **I** is characterized by numerous secondary interactions Au···S and S···Cl between the ionic structural units [52, 53]. So, relatively weak pairwise nonvalent interactions of the first type occur between cations A and C: Au(1)···S(8) 3.6714 Å and Au(3)···S(4) 3.7257 Å, resulting in the formation of linear cationic triads [A···C···A] with the interatomic distance Au(1)···Au(3) 4.0045(2) Å (Fig. 5). In the triads, noncentrosymmetric cations A are antiparallel to each other and the mutual arrangement of cations A and C allows their bisecting planes passing through the $[CS_2AuS_2C]$ bicyclic system to form an angle (80°) close to the right angle. The additional coordination of the sulfur atoms in the axial positions of the gold atoms results in a formal increase in the coordination number of Au(1) to 5 [AuS_{4+1}], and that for Au(3) increases

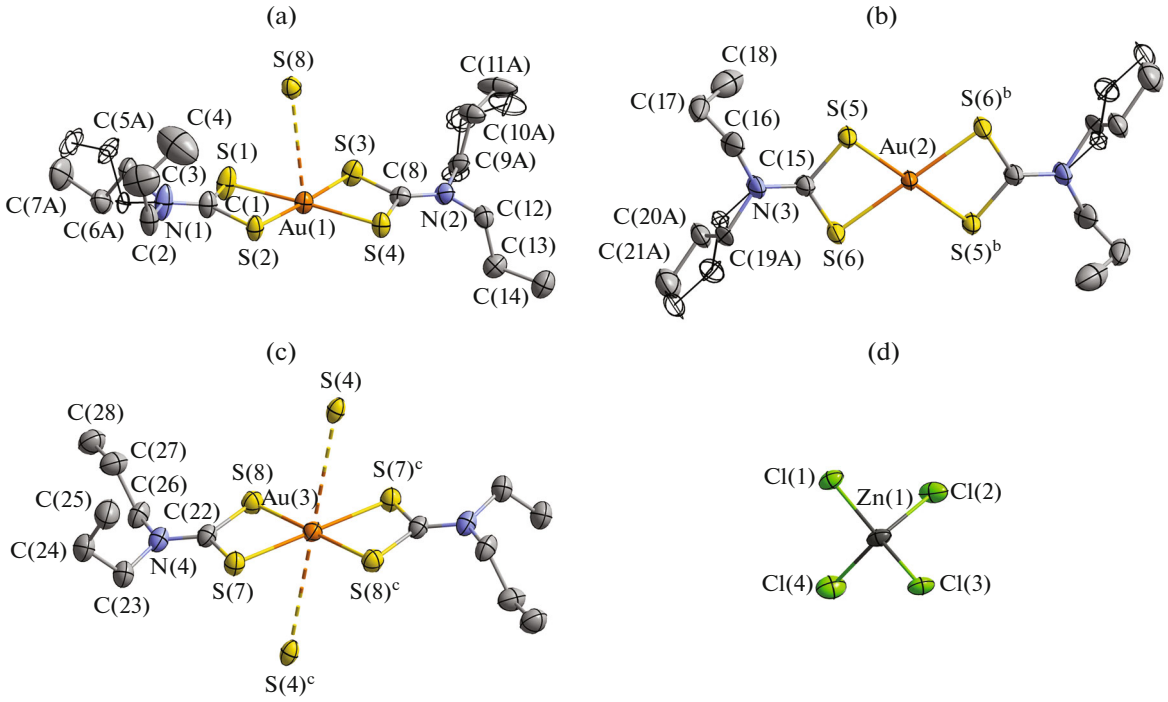

Fig. 3. Structures of three isomeric cations $[Au(S_2CNPr_2)_2]^+$ (a) A, (b), B, and (c) C and (d) anion $[ZnCl_4]^{2-}$in compound **I**. Ellipsoids of 50% probability; uncolored ellipsoids designate randomly disordered carbon atoms in position *B*.

to 6 $[AuS_{4+2}]$ with the building up of the metal polygons to a distorted tetragonal pyramid and an octahedron, respectively (Fig. 5).

In turn, each of isomeric cations B symmetrically interacts with two $[ZnCl_4]^{2-}$ anions to form secondary bonds S(5)···Cl(1)^c and S(5)^b···Cl(1)^d 3.3349 Å, ∠C(15)S(5)Cl(1)^c 170.8(2)°, a consequence of which is the formation of linear anion-cationic triads $\{[ZnCl_4]\cdots B\cdots[ZnCl_4]\}$, whose the Au(2)–Zn(1)^c distance is 6.2188(5) Å (Fig. 5). The anion-cationic triads discussed perform the structural function of double linkers combining the nearest cationic triads due to two pairs of nonsymmetric secondary bonds: Cl(3)$^{c/d}$···S(2)$^{a/e}$ 3.3834 Å, ∠C(1)^{a}S(2)^{a}Cl(3)^c 167.3(1)° and Cl(3)$^{c/d}$···S(4)$^{a/e}$ 3.5045 Å, ∠C(8)^{a}S(4)^{a}Cl(3)^c 171.0(1)°. The overall manifestation of all these secondary interactions leads to the structural ordering of the ionic triads of two types into zigzag (∠Au(3)Au(1)^{a}Zn(1)^c 83.598(5)°) pseudopolymeric ribbons of the $\{\cdots[A\cdots C\cdots A]\cdots[ZnCl_4]\cdots B\cdots[ZnCl_4]\cdots\}_n$ type oriented along the crystallographic *y* axis. The pairwise character of the S···Cl secondary interactions between the linker and each cationic triad predetermines a substantially shorter Au–Zn distance on these regions of the supramolecular ribbon: Au(1)^a–Zn(1)^c 5.6976(4) Å. It should be mentioned that the S···Cl secondary bonds (3.3349–3.5045 Å) are shorter, in all cases, than the sum of the van der Waals radii of the sulfur and chlorine atoms (3.55 Å [50]), and the ∠CSCl angles range from 167.3° to 171.0°. According to the published data [54, 55], the presented structural characteristics make it possible to classify more certainly the interactions discussed as chalcogen (chalcogen–halogen) bonds.

As in the case of compound **I**, the supramolecular structure of compound **II** is formed with the participation of the secondary Au···S and S···Cl interactions supplemented by the C–H···Cl hydrogen bonds (Table 3). Each $[AuCl_4]^-$ anion performs the role of a binding site and thus interacts with four $[Au(S_2CNPr_2)_2]^+$ cations. The most significant pair secondary bonds Cl(1)$^{/a}$···S(2)$^{b/c}$ (3.3200 Å, ∠C(1)S(2)^{b}Cl(1) 168.40(7)°) and Cl(1)$^{/a}$···S(3)$^{b/c}$ (3.2835 Å, ∠C(8)^{b}S(3)^{b}Cl(1) 168.08(8)°) occur between the anion and one of the pairs of the gold(III) cations: the Au–Au distance in the structural fragment Au(1)^b–Au(2)–Au(1)^c is 5.5667(2) Å (Fig. 6). In addition to the diagonal chlorine atoms of the anion, the central gold atom are also involved in the binding with the second pair of cations, which leads to in the appearance of two heterogeneous secondary interactions: Cl(2)$^{/a}$···S(4)$^{/a}$ (3.3730 Å, ∠C(8)S(4)Cl(2) 152.06(7)°) and Au(2)···S(1)$^{/a}$ (3.5302 Å) (the latter somewhat exceeds the sum of the van der Waals radii of gold and sulfur atoms equal to 3.46 Å [50]), deter-

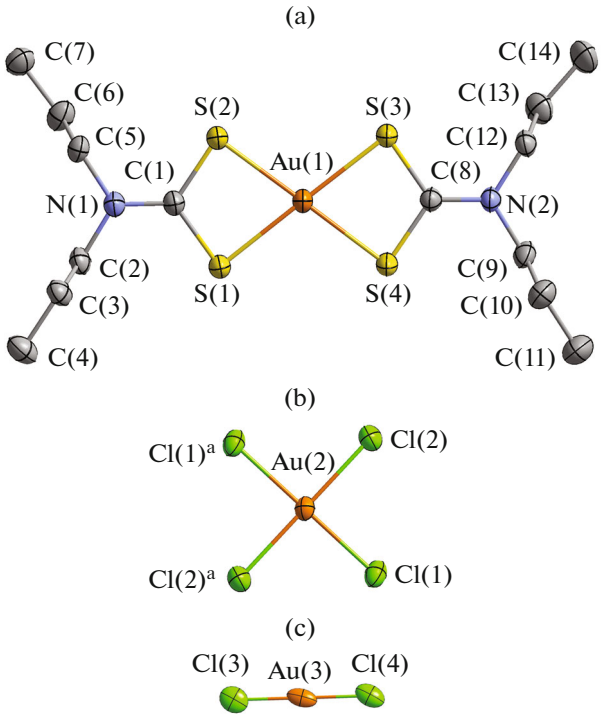

Fig. 4. Structures of the $[Au(S_2CNPr_2)_2]^+$ complex cation (a) and anions $[AuCl_4]^-$ (b) and $[AuCl_2]^-$ (c) in compound **II**. Ellipsoids of 50% probability.

mining a substantially shorter interatomic distance Au–Au (4.6788(2) Å) in the second structural fragment Au(1)–Au(2)–Au(1)[a] (Fig. 6). The described binding mode of the ionic structural units of complex **II** is accompanied by the construction of pseudopolymeric ribbons $\{\cdots[AuCl_4]\cdots 2[Au(S_2CNPr_2)_2]\cdots\}_n$, whose overall stabilization is also contributed by hydrogen bonds C(3)–H(3*B*)···Cl(2)[a] (Fig. 7, Table 3). In turn, the $[AuCl_2]^-$ anions form a system of nonclassical hydrogen bonds C–H···Cl (involving the atoms of the nearest $-CH_2-$ groups in the alkyl substituents of the Pr_2Dtc ligands) and thus combine the discussed supramolecular ribbons into a pseudopolymeric layer (Fig. 7). The geometric parameters of the discussed hydrogen bonds presented in Table 3 are rather typical [56].

The thermal behavior of the synthesized complexes was studied by STA with the simultaneous detection of TG and DSC curves. Compounds **I** and **II** were found to be thermally stable to 178 and 160°C, respectively.

The thermolysis of complex **I** described by the TG curve formally proceeds in two stages (Fig. 8*a*). The main mass loss (54.57%) falls onto the first, steeply descending region of the TG curve (178–348°C), and this value indicates that the thermolysis proceeds at the cation (with the reduction of gold to the elemental state) and anion (with $ZnCl_2$ release). In this variant, the calculated mass loss (59.41%) exceeds the experimental value by 4.84%. Evidently, the second, gentle segment of the TG curve caused by the subsequent gradual evaporation of the thermolysis products can include this missing value. However, the mass loss detected in this case (10.22%) is substantially higher than 4.84% discussed.

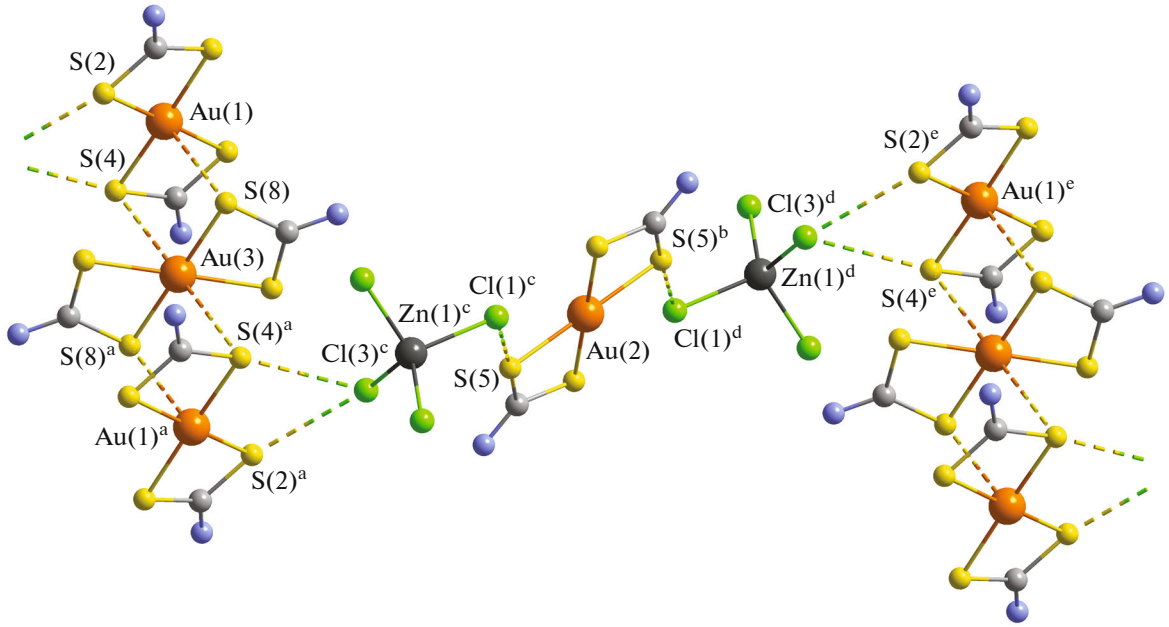

Fig. 5. Supramolecular cation-anionic pseudopolymeric ribbon $\{\cdots[A\cdots C\cdots A]\cdots[ZnCl_4]\cdots B\cdots[ZnCl_4]\cdots\}_n$ of compound **I**. Secondary bonds Au···S and S···Cl are shown by dashed lines. Alkyl substituents are omitted. Symmetry transforms: [a] $-1/2 + x$, $1/2 - y$, $1/2 + z$; [b] $1/2 + x$, $3/2 - y$, $1/2 + z$; [c] $1/2 - x$, $-1/2 + y$, $3/2 - z$; [d] $1/2 + x$, $3/2 - y$, $-1/2 + z$; [e] $3/2 - x$, $1/2 + y$, $1/2 - z$.

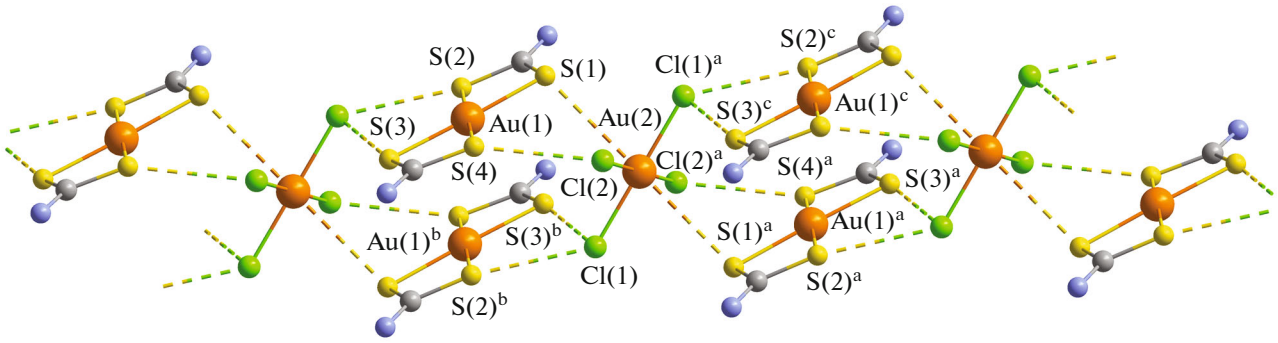

Fig. 6. Formation of the supramolecular pseudopolymeric ribbon $\{\cdots[AuCl_4]\cdots 2[Au(S_2CNPr_2)_2]\cdots\}_n$ of compound **II**. Secondary bonds Au···S and S···Cl are depicted by dashed lines. Alkyl substituents are omitted. Symmetry transforms: [a] $1/2 - x$, $3/2 - y$, $1 - z$; [b] $1/2 - x$, $1/2 - y$, $1 - z$; [c] x, $1 + y$, z.

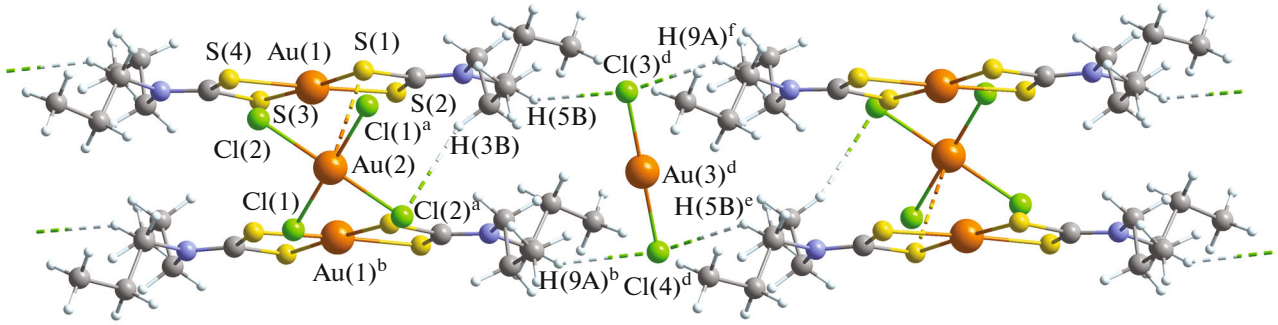

Fig. 7. Joining of the supramolecular ribbons $\{\cdots[AuCl_4]\cdots 2[Au(S_2CNPr_2)_2]\cdots\}_n$ into pseudopolymeric layers involving the $[AuCl_2]^-$ anions. Secondary Au···S bonds and hydrogen C–H···Cl bonds are shown by dashed lines.

To understand reasons for this discrepancy, a set of experimental data on the residual substance will be considered. The weight of the residual substance at 1100°C (34.71% of the initial value) exceeds the weight expected for reduced gold (calcd. 30.15%) by 4.56%. This excessive weight should be assigned to ZnS[1] formed during thermolysis (α/β modification of ZnS is sublimed at 1178/1185°C [58]), which requires 61.13% zinc present in the complex. Thus, the rest 38.87% zinc released in the form of $ZnCl_2$ (T_m/T_b 317/733°C [58]), which composed 4.06% of the initial weight of the complex and evaporated along with other thermolysis products. Reduced gold and a white thin coating of a powdered substance (Fig. 8*c*) were observed on the bottom after the crucible was opened. The powdered substance was studied by the microprobe method. The energy dispersive spectrum of the analyzed sample (Fig. 8*d*), along with the main characteristic peaks of zinc and sulfur, also includes the peaks of gold indicating the presence of microparticles of the latter in identified ZnS.

[1] The formation of metal sulfides upon the thermolysis of the corresponding complexes with the sulfur-containing ligands was substantiated [57] from the thermodynamic viewpoint.

The DSC curve of complex **I** exhibits several endoeffects (Fig. 8*b*). The first of them with an extremum at 169.0°C (the extrapolated T_m = 165.9°C) was attributed to the melting of the complex. The corresponding phase transition was observed at 166–168°C by the independent determination of the melting point of the sample in a glass capillary. The subsequent broadened endoeffect at 247.8°C (the extrapolated temperature 220.4°C) is projected onto the steeply descending region of the TG curve at the point corresponding to the maximum mass loss rate during the intense thermolysis of complex **I**. The endoeffect of melting of reduced gold is detected in the high-temperature region of the DSC curve (the extrapolated T_m = 1062.0°C).

The TG curve of complex **II** (Fig. 9*a*) detects the formally one-stage thermolysis process in a narrow temperature range of ~160–300°C followed by a smooth desorption of volatile decomposition products to 780°C. The regeneration of metallic gold as the single final product in the thermal transformations of the substance is expected. The steeply descending region of the TG curve shows the main mass loss equal to 49.32%, which indicates that the thermolysis of complex **II** proceeds simultaneously at the cation and

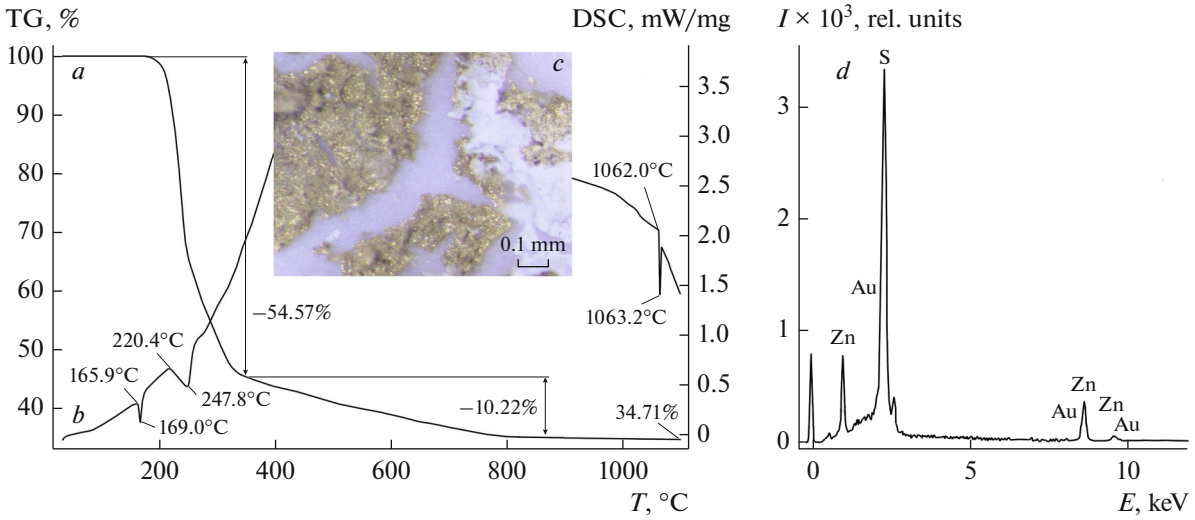

Fig. 8. (*a*) TG and (*b*) DSC curves for complex **I**, (*c*) the enlarged fragment for the crucible bottom with reduced gold and ZnS, and (*d*) the energy dispersive spectrum of ZnS containing reduced gold microparticles.

anions with the reduction of gold(III) and gold(I) to the elemental state.

Before the mass loss onset, the DSC curve of complex **II** (Fig. 9*b*) detects a superposition of the endo- and exoeffects with extrema at 100.6 and 105.1°C, respectively, which can be explained by the transition of the substance to the polymorphic modification stable at elevated temperatures. The subsequent endoeffect at 142.1°C (the extrapolated temperature 139.5°C) is due to the melting of the complex. The independent determination in a glass capillary showed that the melting occurs in a range of 142–144°C. The main mass loss caused by the thermolysis of compound **II** is observed on the DSC curve as an intense endoeffect with an extremum at 280.0°C.

According to the energy dispersive analysis data (Fig. 9*c*), the final product of the thermal destruction of complex **II** is reduced metallic gold for which the DSC curve detects the corresponding endoeffect of melting at 1063.4°C (the extrapolated T_m = 1061.3°C). At 1100°C, the residual weight equal to 45.33% is somewhat underestimated relative to the calculated

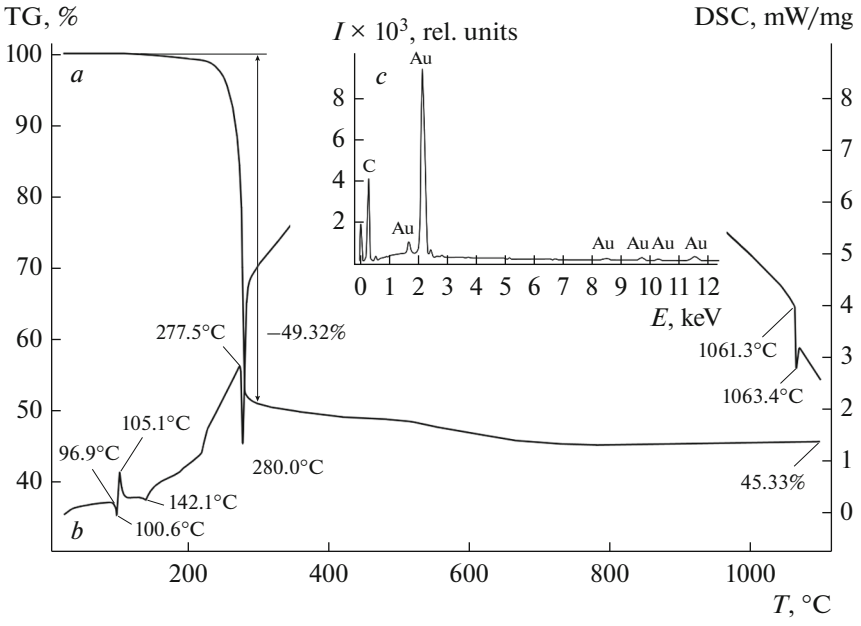

Fig. 9. (*a*) TG and (*b*) DSC curves for complex **II** and (*c*) the energy dispersive spectrum of reduced gold.

value (46.19%). Fine gold balls surrounded by a red-pink sputtering of finely dispersed gold were found on the crucible bottom.

ACKNOWLEDGMENTS

Elemental analysis and IR spectroscopy were carried out using the equipment of the Center for Collective Use of Physical Methods of Investigation at Kurnakov Institute of General and Inorganic Chemistry (Russian Academy of Sciences). The ^{13}C and ^{15}N CP-MAS NMR spectra were recorded at Luleå University of Technology (Sweden) in 2017. Energy dispersive X-ray analysis was carried out at the Center for Collective Use "Amur Center of Mineralogical and Geochemical Studies" of Institute of Geology and Nature Management (Far Eastern Branch, Russian Academy of Sciences).

CONFLICT OF INTEREST

The authors declare that they have no conflicts of interest.

REFERENCES

1. Tiekink, E.R.T., *Crystals*, 2018, vol. 8, no. 7, p. 292.
2. Wyttenbach, A. and Bajo, S., *Anal. Chem.*, 1975, vol. 47, no. 11, p. 1813.
3. Cicotti, M., in *Handbook of Residue Analytical Methods for Agrochemicals*, Lee, P.W., Ed., Chichester: Wiley, 2003, vol. 2, p. 1089.
4. Parny, M., Bernad, J., Prat, M., et al., *Cell Biol. Toxicol.*, 2021, vol. 37, no. 3, p. 379.
5. Len, C., Boulogne-Merlot, A.-S., Postel, D., et al., *J. Agric. Food Chem.*, 1996, vol. 44, no. 9, p. 2856.
6. Nieuwenhuizen, P.J., *Appl. Catal., A*, 2001, vol. 207, p. 55.
7. Anamika, Yadav, C.L., Drew, M.G.B., et al., *Inorg. Chem.*, 2021, vol. 60, no. 9, p. 6446.
8. Fan, H.B., Wang, H.L., Guo, X.P., and Zheng, J.S., *Anti-Corrosion Meth. Mater.*, 2002, vol. 49, no. 4, p. 270.
9. Komatsu, T., *Nippon Gomu Kyokaishi*, 2009, vol. 82, p. 33.
10. Tangavaloo, V., Yuhana, N.Y., and Jiun, Y.L., *Prog. Rubber Plast. Recycl. Technol.*, 2021, vol. 37, no. 4, p. 340.
11. Shi, F., Li, X., Bai, Y., et al., *Appl. Polym. Mater.*, 2021, vol. 3, no. 10, p. 5188.
12. Islam, H.-U., Roffey, A., Hollingsworth, N., et al., *Nanoscale Adv.*, 2020, vol. 2, p. 728.
13. Nyamen, L.D., Nejo, A.A., Pullabhotla, V.S.R., et al., *Polyhedron*, 2014, vol. 67, p. 129.
14. Onwudiwe, D.C., Adeyemi, J.O., Papane, R.T., et al., *Open Chem.*, 2021, vol. 19, p. 1134.
15. Emegha, J.O., Elete, E.D., Efe, F.O., and Adebisi, A.C., *J. Mater. Sci. Res. Rev.*, 2019, vol. 4, p. 1.
16. Snopok, B.A., Zavyalova, L.V., Tatyanenko, N.P., et al., *Mater. Adv.*, 2021, vol. 2, no. 11, p. 3637.
17. Hogarth, G., *Mini-Rev. Med. Chem.*, 2012, vol. 12, p. 1202.
18. Tan, Y.S., Ooi, K.K., Ang, K.P., et al., *J. Inorg. Biochem.*, 2015, vol. 150, p. 48.
19. Irfandi, R., Santi, S., Raya, I., et al., *J. Mol. Struct.*, 2022, vol. 1252. Art. 132101.
20. Ajibade, P.A., Fatokun, A.A., and Andrew, F.P., *Inorg. Chim. Acta*, 2020, vol. 504. Art. 119431.
21. Adeyemi, J.O. and Onwudiwe, D.C., *Inorg. Chim. Acta*, 2020, vol. 511. Art. 119809.
22. Takamune, N., Misumi, S., and Shoji, S., *Biochem. Biophys. Res. Commun.*, 2000, vol. 272, p. 351.
23. Watanabe, K., Kazakova, I., Furniss, M., and Miller, S.C., *Cell. Signal*, 1999, vol. 11, p. 371.
24. Lang, J.-M., Trepo, C., Kirstetter, M., et al., *Lancet*, 1988, vol. 332, p. 702.
25. Ivanov, A.V., Loseva, O.V., Rodina, T.A., et al., *Russ. J. Inorg. Chem.,* 2014, vol. 59, no. 8, p. 807. https://doi.org/10.1134/S0036023614080105
26. Ivanov, A.V., Rodina, T.A., and Loseva, O.V., *Russ. J. Coord. Chem.*, 2014, vol. 40, no. 12, p. 875. https://doi.org/10.1134/S1070328414120069
27. Loseva, O.V., Rodina, T.A., and Ivanov, A.V., *Russ. J. Coord. Chem.*, 2013, vol. 39, no. 6, p. 463. https://doi.org/10.1134/S1070328413050060
28. Rodina, T.A., Loseva, O.V., Smolentsev, A.I., and Ivanov, A.V., *J. Struct. Chem.*, 2016, vol. 57, no. 1, p. 146. https://doi.org/10.1134/S0022476616010182
29. Rodina, T.A., Loseva, O.V., and Ivanov, A.V., *J. Struct. Chem.*, 2021, vol. 62, no. 1, p. 123. https://doi.org/10.1134/S0022476621010157
30. Loseva, O.V., Rodina, T.A., and Ivanov, A.V., *Russ. J. Inorg. Chem.,* 2015, vol. 60, no. 3, p. 307. https://doi.org/10.1134/S0036023615030134
31. Loseva, O.V., Rodina, T.A., Ivanov, A.V., et al., *Russ. J. Coord. Chem.*, 2018, vol. 44, no. 10, p. 604. https://doi.org/10.1134/S107032841810007X
32. Byr'ko, V.M. *Ditiokarbamaty* (Dithiocarbamates), Moscow: Nauka, 1984.
33. Sreehari, N., Varghese, B., and Manoharan, P.T., *Inorg. Chem.*, 1990, vol. 29, p. 4011.
34. Ivanov, A.V., Ivakhnenko, E.V., Gerasimenko, A.V., and Forsling, W., *Russ. J. Inorg. Chem.*, 2003, vol. 48, no. 1, p. 45.
35. Afanas'eva, V.A., Glinskaya, L.A., Klevtsova, R.V., and Mironov, I.V., *Russ. J. Coord. Chem.*, 2011, vol. 37, no. 5, p. 325.
36. APEX2. Madison (WI, USA): Bruker AXS Inc., 2012.
37. Sheldrick, G.M., *Acta Crystallogr., Sect. A: Found. Adv.*, 2015, vol. 71, no. 1, p. 3.
38. Sheldrick, G.M., *Acta Crystallogr., Sect. C: Struct. Chem.*, 2015, vol. 71, no. 1, p. 3.
39. Pines, A., Gibby, M.G., and Waugh, J.S., *J. Chem. Phys.*, 1972, vol. 56, no. 4, p. 1776.
40. Earl, W.L. and Vanderhart, D.L, *J. Magn. Reson.*, 1982, vol. 48, no. 1, p. 35.
41. Morcombe, C.R. and Zilm, K.W., *J. Magn. Reson.*, 2003, vol. 162, no. 2, p. 479.
42. Ratcliffe, C.I., Ripmeester, J.A., and Tse, J.S., *Chem. Phys. Lett.*, 1983, vol. 99, no. 2, p. 177.

43. Bellamy, L.J., *The Infrared Spectra of Complex Molecules*, New York: Wiley, 1958.
44. Casas, J.S., Sánchez, A., Bravo, J., et al., *Inorg. Chim. Acta*, 1989, vol. 158, no. 1, p. 119.
45. Yin, H., Li, F., and Wang, D., *J. Coord. Chem.*, 2007, vol. 60, no. 11, p. 1133.
46. Nakamoto, K., *Infrared Spectra and Raman Spectra of Inorganic and Coordination Compounds*, New York: Wiley, 1986.
47. Rodina, T.A., Loseva, O.V., Smolentsev, A.I., et al., *Inorg. Chim. Acta*, 2020, vol. 508. Art. 119630.
48. Korneeva, E.V., Smolentsev, A.I., Antzutkin, O.N., and Ivanov, A.V., *Inorg. Chim. Acta*, 2021, vol. 525, Art. 120383.
49. Pauling, L., *The Nature of the Chemical Bond and the Structure of Molecules and Crystals*, London: Cornell Univ., 1960.
50. Bondi, A., *J. Phys. Chem.*, 1964, vol. 68, no. 3, p. 441.
51. Yang, L., Powel, D.R., and Houser, R.P., *Dalton Trans.*, 2007, vol. 9, p. 955.
52. Alcock, N.W., *Adv. Inorg. Chem. Radiochem.*, 1972, vol. 15, no. 1, p. 1.
53. Haiduc, I. and Edelmann, F.T., *Supramolecular Organometallic Chemistry*, Weinheim: Wiley, 1999.
54. Wang, W., Ji, B., and Zhang, Y., *J. Phys. Chem.* A, 2009, vol. 113, no. 28, p. 8132.
55. Scilabra, P., Terraneo, G., and Resnati, G., *Acc. Chem. Res.*, 2019, vol. 52, no. 5, p. 1313.
56. Bakhtiyarova, Y.V., Aksunova, A.F., Galkina, I.V., et al., Russ. Chem. Bull. Int.. Edit., 2016, vol. 65, no. 5, p. 1313.
57. Razuvaev, G.A., Almazov, G.V., Domrachev, G.F., et al., Dokl. Akad. Nauk SSSR, 1987, vol. 294, p. 141.
58. Lidin, R.A., Andreeva, L.L., and Molochko, V.A. Spravochnik po neorganicheskoi khimii (Reference Book in Inorganic Chemistry), Moscow: Khimiya, 1987.

Translated by E. Yablonskaya